Check for updates

ADVANCED MATERIALS TECHNOLOGIES
www.advmattechnol.de

A Hybrid Upper-Arm-Geared Exoskeleton with Anatomical Digital Twin for Tangible Metaverse Feedback and Communication

Minhyeok Ha, Jihun Lee, Yongbeom Cho, Minwoo Lee, Hyunwoo Baek, Jungmin Lee, Jongmin Seo, Sejoon Chun, Kisoo Kim, Jin-Gyun Kim,* and Won Gu Lee**

The pandemic coincided with rapid advancements in virtual reality (VR) and mixed reality (MR) in healthcare. The idea of virtually replicating the real world and its associated experiences has garnered significant attention under the newly coined term "metaverse." The metaverse serves as a communication platform that integrates physical and virtual experiences. However, the lack of physical interaction between users and virtual environments remains an obstacle. This study introduces a hybrid upper-arm-geared exoskeleton system that combines an anatomical digital-twin model with tangible VR torque feedback and an MR remote healthcare monitoring in a musculoskeletal interface device format. The device employs a dual epicyclic geared motor actuator capable of exerting torque feedback. It derived torque profiles that simulate physical interactions with hysteretic damping in the virtual environment. An anatomical digital twin model is also incorporated into the fabricated device in an MR format and assessed the device's performance using electromyogram and thermographic sensors. In addition, it evaluated haptic fidelity and versatility as an immersive metaverse wearable and performed support vector machine-based analysis for motion feature classification. It believes this approach has the potential to be highly beneficial for providing tangible metaverse feedback and communication combined with a human-informed digital-twin model for remote healthcare monitoring in the postpandemic era.

1. Introduction

Patients with musculoskeletal disorders require physical rehabilitation to restore functions, improve range of motion, and reduce pain. The guidance of a professional is required for feasible, safe, and efficacious rehabilitation.[1] The COVID-19 pandemic, which began in 2019, increased the demand for remote rehabilitation technologies as an alternative means of rehabilitation in the physical environment for adhering to social distancing measures.[2,3] While remote communication can guide rehabilitation, the lack of physiological information about the patient can limit its effectiveness.[3,4] Wearable human–machine interface devices can evaluate the movement of patients and assess their risk in remote training.[5,6] Patients requiring physical rehabilitation can also experience assistance through immersive training within a virtual reality environment, offering a unique and practical approach to treatment.[7] However, previous remote rehabilitation platforms have limitations in that the device offers only individual training without accurate guidance due to the lack of information delivered to experts.

Wearable exoskeletons have been introduced to assist with walking, climbing stairs, feeding themselves, and participating in rehabilitation.[8,9] Exoskeletons, or wearable robotics, are designed to augment, support, or enhance human physical abilities through sensory and actuation systems.[10–12] However, these exoskeletons typically entail high costs and complex data processing to accurately track the human body's multi-dimensional motions.[13] The conventional motion tracking methods through the wearable exoskeletons provide complex location data for precise posture control, which requires high computing power and numerous sensors. The high cost of exoskeletons makes remote rehabilitation challenging, and the previously available lower-priced exoskeletons have had limitations in providing sufficient support for expert rehabilitation guidance due to a lack of transferability of information and physical forces between real and virtual worlds.[14]

M. Ha, J. Lee, M. Lee, J. Lee, J. Seo, S. Chun, W. G. Lee
Department of Mechanical Engineering
Kyung Hee University
Yongin 17104, Republic of Korea
E-mail: termylee@khu.ac.kr

Y. Cho, H. Baek, J.-G. Kim
Department of Mechanical Engineering (Integrated Engineering)
Kyung Hee University
Yongin 17104, Republic of Korea
E-mail: jingyun.kim@khu.ac.kr

K. Kim
Intelligent Optical Module Research Center
Korea Photonics Technology Institute (KOPTI)
Gwangju 61007, Republic of Korea
E-mail: kisookim@kopti.re.kr

The ORCID identification number(s) for the author(s) of this article can be found under https://doi.org/10.1002/admt.202301404

DOI: 10.1002/admt.202301404

 © 2023 Wiley-VCH GmbH

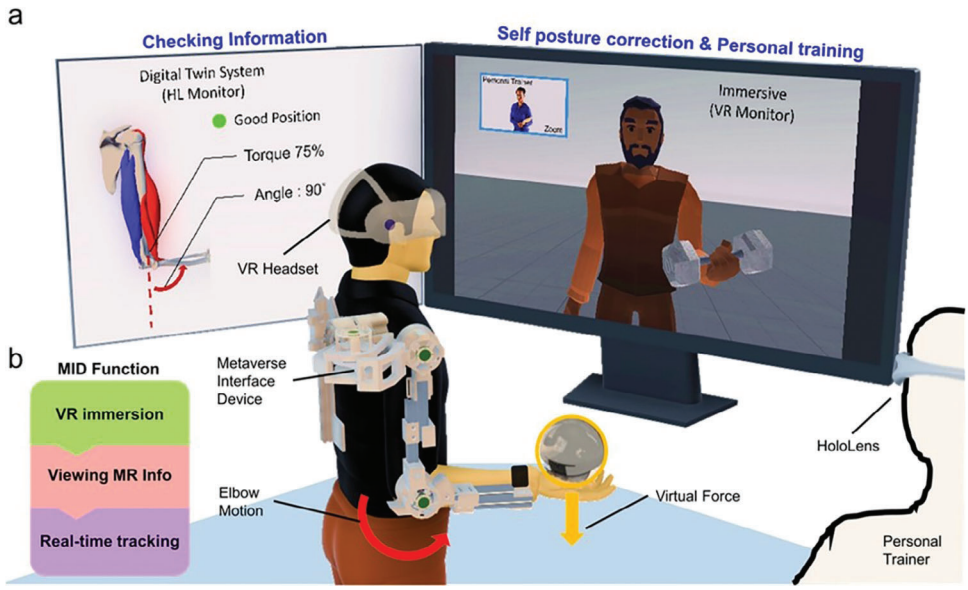

Figure 1. Schematic illustration of a hybrid upper-arm guided exoskeleton (hUGE) system that can combine immersive torque feedback with a digital anatomical muscle model for remote healthcare monitoring between trainer and trainee. a) Showcased illustration for a device operation with torque feedback, displaying elbow motion (of trainee) and personal training feedback (by a trainer), along with hybrid virtual reality (VR) monitoring (in metaverse) and MR display (via a Hololens). b) The three primary functions of the MID are VR immersive feedback, MR informative interaction, and real-time tracking in a digital twin format.

A digital twin is a technique that augments virtual simulation information to improve the accuracy of decisions, and a metaverse interface that utilizes augmented reality (AR), virtual reality (VR), and mixed reality (MR) technology can enhance the immersive experience of digital twins.[15–18] Digital twin technologies can also be used in various applications, ranging from medical operations,[19–21] and surgical training[22] to rehabilitation.[23] The digital twin healthcare systems, which provide feedback on a variety of information, are continuously evolving to enhance monitoring, control, and decision support.[24,25] Physical interaction and feedback with physiological signals are key parameters connected to the virtual world for remote healthcare systems, and digital twin technology can augment those data to help experts make accurate decisions in a remote environment.

This study proposes and implements a hybrid upper-arm geared exoskeletal (hUGE) system that enhances muscle response with tangible torque interaction for personalized rehabilitation in a musculoskeletal interface device (MID) format (**Figure 1a**). The MID corresponds with the motions of the elbow and shoulder with a virtual platform through physical motor control feedback. The system features a brushless DC (BLDC) motor with an epicyclic gearbox for generating torque, which implements various angular movements. A magnetic rotary encoder sensor collects joint rotation angles to reflect the virtual environment. We evaluated the electromyogram (EMG) signals of participants wearing the MID to analyze the effects on muscles during various movements. The MID aims to enhance the immersion and interactivity of users in the virtual environment. Thus, we designed and evaluated exoskeletal devices that detect motion for elbow and shoulder joints and output appropriate torque to the user through actuators. We also analyzed the MID's thermal behavior and performed mechanical simulation to ensure reliability and safety. The MID offers an immersive experience by providing a real-time tracking anatomical digital twin model that augments muscle movement for rehabilitation on a virtual platform (Figure 1b). A personal trainer can offer feedback on rehabilitation based on the anatomical digital twin model, and the MID has the potential to better measure, track over time, and optimize physical rehabilitation procedures and patient outcomes.

2. Experimental Section

In this section, the design and implementation of the exoskeleton are described. The exoskeleton consists of an actuator using a BLDC motor with a gear train that provides an output torque equivalent to holding up to 1 kg of weight. The structural component of the exoskeleton was made of an aluminum extrusion profile and a 3D-printed structure, and it was designed to operate within a safe range of motion for the user's elbow joint. The shoulder joint had three degrees of freedom (DOF) and could rotate. In addition, the exoskeleton was intended to provide physical feedback to the user through torque output using motor control.

The MID implemented as an exoskeleton employed the BLDC motors and actuators using a dual planetary gearbox with a gear ratio of ≈47, which enables the device to generate the torque equivalent of lifting a weight of ≈3 kg at a 0.3 m distance from the elbow to the wrist (Figure S1a, Supporting Information). Utilizing a link design, the exoskeleton's joints were designed considering the human body's rotational limitations and shoulder rotation axis characteristics. The structural components comprised 3D printed structures and aluminum profiles (Figure S1b, Supporting Information). This design, which considers the rotational limits of the human body, prevented reverse rotation

© 2023 Wiley-VCH GmbH

2365709x, 2024, 2, Downloaded from https://onlinelibrary.wiley.com/doi/10.1002/admt.202301404 by Kyung Hee University Library, Wiley Online Library on [19/11/2024]. See the Terms and Conditions (https://onlinelibrary.wiley.com/terms-and-conditions) on Wiley Online Library for rules of use; OA articles are governed by the applicable Creative Commons License

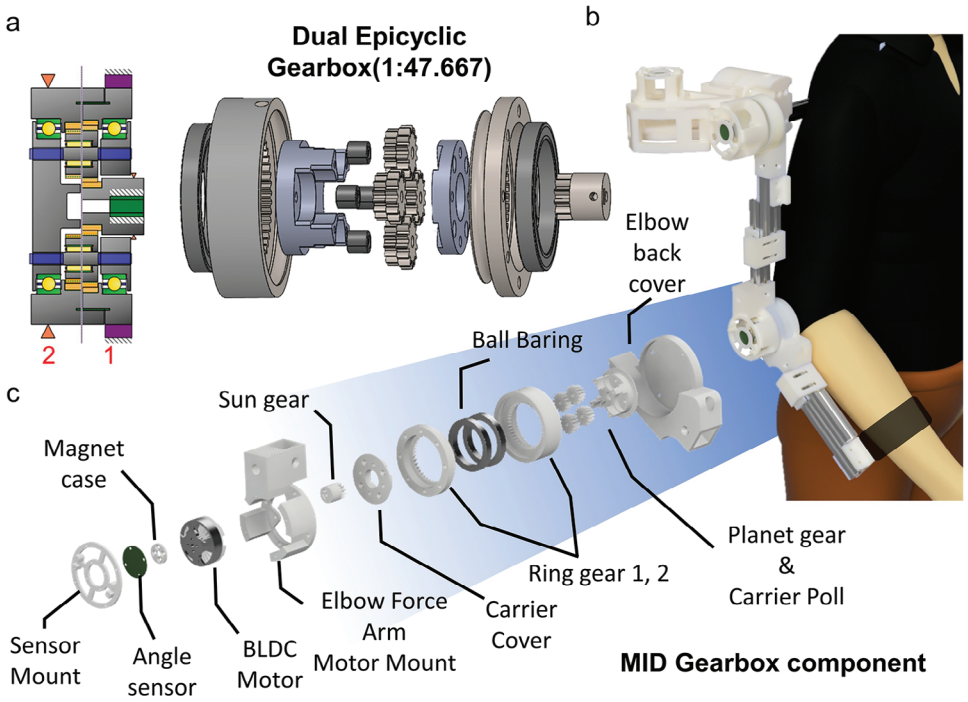

Figure 2. Configurational setup and loaded tooth contact analysis (LTCA) of the reduction gearbox. a) The assembled gearbox, b) Cartoon for the wearable format, c) Design and configuration details. The device consists of three shoulder joints and a single elbow joint, and each joint is embedded in a dual epicyclic gearbox (1:47.667) with BLDC Motor (4108MR-380KV).

of the user's elbow joint, ensuring operation within a safe range of motion. The shoulder joint possessed three DOFs and could rotate. Real-time torque control uses the exoskeleton's motor to provide the user with physical feedback and therapeutic resistance.

2.1. Design Principles and Key Assembly Considerations of a Metaverse Wearable with Tangible Torque Feedback

As robots increasingly assist human activities and become integrated into daily life, the importance of human–robot interaction is becoming paramount. Exoskeleton systems facilitate human–robot interactions, necessitating compliance control designs that adapt to the surrounding environment. However, traditional robotic actuators, which connect high-speed, low-torque motors to high-gear ratio reducers, achieve high torque density at the expense of being difficult (high impedance) to rotate under external input. To address these challenges, various existing exoskeleton systems widely employ series elastic actuators (SEAs) that improve the overall adaptability of the actuator to external environments. SEAs utilized a mechanically compliant layer that was elastically coupled to high-impedance actuators, allowing them to adapt to external movements.

Furthermore, an additional control approach was introduced based on the discrepancies between the movements, further enhancing the actuator's adaptability to its surroundings.[26] However, the utility of SEAs decreased when applied to rehabilitation applications. Recently, a (quasi-)direct drive approach was proposed for small-scale walking robots that employ large-diameter BLDC motors with relatively low gear ratios. This approach allowed lightweight, compact actuators adapted to external environments while implementing dynamic actions. As the approach requires lightweight and compact actuators in exoskeleton systems and the performance demands in various external force situations encountered during activities of daily living (ADL), direct drive methods were increasingly adopted in various exoskeleton systems.[27,28] Utilizing these principles, the system implemented a quasi-direct drive actuator by connecting a commercial BLDC motor with the appropriate gear ratio to a 3D-printed planetary gear produced with rapid prototyping.

2.1.1. Motor-Geared Joint Actuators

The hardware frame, which directly contacts and controls the human body, was designed considering the same DOF as the human body, based on ergonomic knowledge. The ergonomic design and the required DOF for actuating the joints of the elbow and shoulder, excluding the hand, include three DOF (roll, pitch, and yaw angles) for the shoulder and one DOF (rotation) for the elbow, which were taken into account during the hardware frame design process. A total of three motor drives were implemented for torque feedback through the parallel four-bar linkage when creating the shoulder exoskeleton, and one motor was placed at the elbow to transmit the forces of the biceps, forearm, and triceps, using a total of four motor reducers (**Figure 2a**).

The upper-limb exoskeleton was one DOF in the plane, allowing rotation in the YZ plane based on the *x*-axis. Although the elbow was two DOF, including forearm rotation, the MID

© 2023 Wiley-VCH GmbH

2365709x, 2024, 2, Downloaded from https://onlinelibrary.wiley.com/doi/10.1002/admt.202301404 by Kyung Hee University Library, Wiley Online Library on [19/11/2024]. See the Terms and Conditions (https://onlinelibrary.wiley.com/terms-and-conditions) on Wiley Online Library for rules of use; OA articles are governed by the applicable Creative Commons License

focused on the contraction and relaxation of the forearm, biceps, and triceps muscles through *x*-axis rotation and was designed using a single motor for one DOF. The shoulder exoskeleton deviates from the conventionally used three-DOF joints by positioning the *y*-axis revolute joint from the top of the shoulder to the back and placing the *z*-axis in the diagonal outer space of the shoulder, preventing collisions between the exoskeleton and the human body during movement. A double parallelogram linkage was used here, which connects two rotating joints to implement motion like a spherical joint while maintaining a remote center of rotation. This linkage had an extensive range of motion (ROM) and high overall stiffness and was advantageous for exoskeleton applications due to its suitable size and lightweight construction.

2.1.2. Motor Reducer Design and Specification

In order to exert a force of 3 kg with a BLDC motor, the end effector should support a load of 30 N. At this point, ≈9 N m of torque was required at the elbow. Therefore, the motor output torque of 0.2 N m should be amplified by a factor of 47 to derive 9 N m when a maximum continuous applied current of 10 A was given to the BLDC motor. This 46-fold value determined the necessary number of teeth for each component in the double planetary gear system using "*David Hartkop*'s" formula (also known as a split-ring compound-planet epicyclic gear system), and the gearbox was subsequently fabricated. The motor reducer was a split-ring compound-planet epicyclic gear, a "Wolfrom," and a "3K" planetary gearbox. The reducer was composed of a total of four planet gears (first and second stage), one sun gear (first stage), two ring gears (first and second stage), and two carriers. The number of teeth for each gear was 14 for the first and second-stage planet gears, 12 for the sun gear, 40 for the first-stage ring gear, and 44 for the second-stage ring gear. This was developed by referencing the resulting values obtained by inputting the required torque amplification of ≈47 into "*David Hartkop*'s" formula. A commercial ODrive motor controller board, equipped with a three-phase converter circuit, microprocessor, and other electronic circuits, was adopted to drive the BLDC motor. A magnetic rotary encoder sensor obtains the high-resolution real-time motor rotation angle data required for driving. Voltage, current, and torque could be measured through the ODrive v3.6 motor controller board. After configuring the ODrive board for the desired motor environment, the input voltage could be checked using a command. The electric current check command could also determine the torque applied to the motor. The values obtained through ODrive were transmitted wirelessly to Unity via a Raspberry Pi Pico and graphed in Excel. In a static equilibrium situation where the upper limb's end effector supports a 30 N (almost the same as 3 kg) load, the moment at the elbow joint corresponds to ≈9 N m. This was intended to amplify the motor output torque of ≈0.2 N m by 40 times when the maximum continuous applied current (thermally limited with passive cooling through the aluminum frame) of 10 A was given to the desired BLDC motor. In a compact form, the "Wolfrom" and "3K" planetary gearboxes could implement a more significant reduction ratio than conventional planetary gears (≈1:10).[29] To evaluate the fabricated device, static measurements were conducted using strain gauges.

2.2. Loaded Tooth Contact Analysis (LTCA) of a Reduction Gearbox for Tangible Torque Generation and Its Feedback

The reduction gearbox should be designed considering structural strength concerning the operating conditions. To verify the strength and robustness of the components, which consist of the reduction gearbox, safety factor calculation using simulations was conducted in this work. A loaded tooth contact analysis (LTCA) for the reduction gearbox was conducted as a numerical analysis for the simulation method. LTCA was a widely used method to predict the bending and contact stress at the tooth.[30] It considered the engagement of the tooth as quasi-static with each contact position due to the rotating and contact convergence. However, dynamic behavior such as time-transient force and response was not considered because this had less effect on the result, especially at low rotating speeds. This work uses the commercial software *MASTA* to generate the LTCA simulation model, as shown in Figure 2. The LTCA results will be discussed in Section 3.3. The reduction gearbox design described in Section S1 (Supporting Information) and the macro geometries of the planetary gearsets are summarized in Table S1 (Supporting Information). The other design parameters follow the ISO 21771 and ISO 53 standards. However, micro geometry modification was not considered for this research. The shafts and body models were generated regarding the gearbox CAD modeling. The gears and shafts use polylactic acid(PLA) mechanical materials, with their properties listed in Table S2 (Supporting Information). The stiffness matrices of the bearings were generated using the MASTA library provided by the bearing manufacturers. The output torque position was set on the second stage annulus gear body assembled with the elbow forearm, and the input torque was applied at the first stage sun gear shaft connected with the BLDC motor shaft. The load cases of the LTCA simulation are summarized in Table S3 (Supporting Information).

2.3. Modeling of Anatomical Digital Twin Model for Hololens-Based Monitoring

A digital twin was a virtual replica created to reflect an actual model. Combining the digital twin concept with metaverse environments could produce robust visualization tools for rehabilitation medicine that could not be demonstrated in the actual world without invasive procedures. This study developed a real-time VR and MR framework of an anatomical model activated by the exoskeleton model. The suggested architecture provided various rehabilitation monitoring data, including muscle relaxation, muscle contraction, motor torque, etc. A digital twin refers to a virtual counterpart that operates identically to the physical entity, enabling the visualization of movements that could not be observed in reality. This study uses a "*HoloLens*" device to visualize muscle and MID information in real-time within an MR environment. An MR environment was one in which the user could physically interact with digital AR or VR components. If a personal trainer utilized this for monitoring a MID wearer, they could provide feedback on the exercise status using information such as muscle contraction levels or generated torque. Importantly, this MR exoskeleton could enable physical trainers and healthcare professionals to track and optimize patient progress

© 2023 Wiley-VCH GmbH

2365709x, 2024, 2, Downloaded from https://onlinelibrary.wiley.com/doi/10.1002/admt.202301404 by Kyung Hee University Library, Wiley Online Library on [19/11/2024]. See the Terms and Conditions (https://onlinelibrary.wiley.com/terms-and-conditions) on Wiley Online Library for rules of use; OA articles are governed by the applicable Creative Commons License

in a controlled manner quantitatively. With an improved ability to measure exercise, there was a potential to optimize exercises better.

2.4. Exercise Efficacy Testing Using Electromyographic (EMG) Sensors

The need for EMG measurement arises from the limitations of conventional haptic devices or VR devices, which lack immersion due to the absence of counter-rotation (torque feedback) when interacting with virtual objects. However, the MID developed in this study was designed to enable physical interaction with virtual objects by providing torque feedback, increasing the immersion level. Therefore, a measurement experiment was conducted to verify whether the force generated during bicep curl movements when wearing the MID was similar to that of actual bicep curls. The rationale for the time setting was that muscles do not continuously exert maximum force; instead, they generate maximum force at the moment they exert maximum contraction. Furthermore, applying force to the muscles for an extended period may hinder muscle activity measurement due to muscular endurance. Therefore, an appropriate balance between resting and exercise time was necessary for effective electromyography measurement. Therefore, the time intervals were set to rest from 0 to 5 s, 10 to 20 s, and 25 to 35 s, and perform bicep curl movements from 5 to 10 s, 20 to 25 s, and 35 to 40 s.

The selected weights were chosen because older individuals and patients undergoing rehabilitation needed to be given appropriate weights to strengthen elbow muscles for rehabilitation purposes. The individual's muscle strength level should be considered when selecting the weight to achieve appropriate rehabilitation. The chosen weights may not be suitable for older individuals or rehabilitation patients with relatively low muscle strength and endurance; however, these weights fall within the range of objects typically used in everyday life. This experiment aims to verify the similarity of movements while wearing the MID to actual bicep movements; therefore, using 5 kg as the maximum weight, with 2.5 kg as half of that, and 1 kg as a relatively more minor weight was experimented. Consequently, for each weight, 1 kg was light and offered low resistance, enhancing muscle endurance and making it suitable for early-stage rehabilitation. It may be a particularly appropriate choice for older individuals and rehabilitation patients with weak muscle strength. A moderate weight was 2.5 kg, capable of simultaneously improving muscle strength and endurance. This weight may be suitable for those past the initial rehabilitation stage or older individuals and rehabilitation patients with relatively higher muscle strength. Finally, 5 kg provided high resistance, aiding in increasing muscle strength. This weight may be appropriate for middle-to-late-stage rehabilitation or relatively healthy older individuals.

The program used to receive and analyze the EMG values is "*Telescan*." The electromyography values were measured and stored in real-time for the experiment, and the results were refined by setting a range of 10–400 with a bandpass filter and applying a root mean squared (RMS) value of 100. The instrument (LAXTHA's WEMG-8, LXM5308) measuring the EMG signals could measure wireless electromyography across eight channels within a radius of 30 meters. The EMG measurement equipment comprises a receiver and a transmitter (as a connection box). The receiver was connected to a laptop for power supply, and the transmitter had a ground electrode connector and a signal electrode connector. The ground electrode connector was used to attach a sensor for grounding, and the signal electrode connector was used to attach the EMG sensor. The signal electrode connector could connect two EMG electrodes to a single connector, and the EMG electrodes were attached based on the location where the muscle density was highest when the force was applied perpendicular to the muscle fibers.

2.5. Thermographic Imaging and Analysis

The MID generates load through the BLDC motor, and the gearbox counter-rotates to create the necessary feedback for the given interaction. The gearbox coupling part (i.e., body contact portion) came into contact with the wearer's skin when the MID was worn. The heat generated by the motor load could harm the human body, like burns; therefore, a thermal safety evaluation test was essential through thermal imaging experiments. Additionally, the thermal imaging evaluation was necessary to reduce the chance of damage to the machinery. Rapid temperature increases in the motor due to factors such as current overload, short circuits, or frame snagging while driving the BLDC motor could cause problems with MID operation and potentially lead to more significant accidents.

An infrared camera (FLIR E8-XT) was used to measure the heat generated by the MID. To prevent external factors from interfering, it conducted experiments in a room of ≈35 m^2 while maintaining a constant temperature (≈20°C). The thermographic imaging experiment was conducted by connecting the equipment to a laptop and performing real-time thermal analysis using FLIR Thermal Studio. The software was used to measure and convert the temperature changes of the motor and the surrounding frame in real-time into images as the motor operating time varied. The images visualized the temperature distribution of the motor and frame, the temperature distribution map, and the temperature of a specific, focused area.

Thermal imaging measurements were conducted at the BLDC motor coupled to the gearbox and the part of the MID that touches the elbow. The first location was chosen because the BLDC motor generates heat through counter-rotation as it creates torque feedback for the physical force in the virtual environment due to the gearbox ratio and the interaction with Unity's weight-setting mass value. The second location, the body contact part, was chosen to measure the heat generated by the BLDC motor, which directly touches the skin, and to determine whether the temperature may be hazardous. In particular, it focused on measuring the temperature of the copper inside the BLDC motor. The temperature of the copper provides information about the motor's safety and lifespan. Moreover, the temperature inside the motor was more likely to increase when there were sudden changes in rotation direction or repeated stops; in such cases, the copper's temperature rose first, which was why it was chosen as the measurement spot.

© 2023 Wiley-VCH GmbH

2365709x, 2024, 2, Downloaded from https://onlinelibrary.wiley.com/doi/10.1002/admt.202301404 by Kyung Hee University Library, Wiley Online Library on [19/11/2024]. See the Terms and Conditions (https://onlinelibrary.wiley.com/terms-and-conditions) on Wiley Online Library for rules of use; OA articles are governed by the applicable Creative Commons License

2.6. Classification of Subtle Movement Variations through the Support Vector Machine Algorithm

In this section, precisely classified individuals with subtly different movements using a machine learning technique called the Support Vector Machine (SVM). There were several differences between SVM and various deep learning techniques when viewed from the perspective of prediction outcomes. These differences include model complexity, data size, feature engineering, degree of fit, interpretability, and training capabilities. In this context, the SVM technique was chosen for its ability to accurately classify categorical data obtained from specialized small-group experiments, thus validating the proof-of-concept demonstration of the device. Five participants were involved in the experiment, and they were labeled from E1 to E5, in descending order of muscle strength, as determined through measurement. The subjects wore devices and performed a continuous set of 20 bending and stretching movements, from which data were collected. The acquired data were divided into a ratio of 4:1 for the respective training and testing datasets, and the accuracy was verified by comparing the model's predicted data with the test data. During this process, it engaged in accurate learning and classification by altering various kernel functions and the c and gamma parameter values and analyzed the distribution of each participant's dataset for a precise diagnosis of movement. The c value indicates the degree to which positioning in a different class was allowed during classification, and the gamma value signifies the sensitivity to the training data. Consequently, higher c and gamma values enable highly accurate classification within the training data, although they also increase the likelihood of overfitting errors and the possibility of less accurate classification concerning the test data. Therefore, in this experiment, an accurate model was identified by comparing the accuracy of the training and test data.

2.7. Clinical Studies

This study was approved by Kyung Hee University's Institutional Review Board under the trial registration number KHGIRB-22-423. The experiment was conducted after obtaining the informed consent of all participants. The participants had described experiments including consecutive bending-stretching movements and then performed the same movements. The purpose of the preclinical test was to evaluate the usability and safety of wearable devices.

3. Results and Discussion

3.1. Implementation of a Haptic Device Interfaced for Metaverse Feedback and Communication in an MR Format

Unity (a popular 3D physical game engine) was used to implement VR virtual space, user avatars, and physical interaction simulation. The user's arm posture is estimated based on the elbow or shoulder rotation angle through the device sensor, and the experimental evaluation is modeled by giving three general load conditions according to the physical interaction context in a virtual environment. The torque of the equivalent-size matched units for the virtual set is the physical amount based on the voltage-to-torque characteristics of the actuator previously determined through measurement. The torque value calculated accordingly was given to the actual device (Figure S1c, Supporting Information). MID offers the output of the torque value considering the object's weight and the arm's length and the differential implementation of torque proportion and weight. The algorithm explains the feedback that the user will receive for the three different weight conditions. However, this torque feedback experience was limited to the elbow, and shoulder motion is measured through a printed circuit board and linked with the Unity avatar. The three conditions have limitations in including all practical experiences and work simulations in the actual industry, but the evaluated data will be able to simulate appropriate situations.

3.1.1. MR-Based Combination of the Metaverse Exoskeleton and Anatomical Digital Twin Model

To combine the anatomical muscle model with the MID wearable, we used digital prototypes for both the exoskeleton device and the human arm model, which is the subject of rehabilitation. The exoskeleton device is designed to support the torque necessary to assist in curl exercises. We imported a 3D CAD model into Blender SW and converted it into a kinematics-based model to implement the digital twin of the exoskeleton. The digital twin of the human arm model is designed to acquire anatomical data of the biceps and triceps, which are mainly stimulated during curl exercises. We utilized a model from "*BodyParts3D*,"[31] which provides various human body shape data, and we accurately simulated the movement of joints and muscles through rigging work. The human arm digital twin model can represent the contraction of the biceps and relaxation of the triceps when lifting weight and restoring to its original state during the opposite motion. The human arm digital twin model is developed to operate in real-time, synchronized with the measured angle acquired through MID's encoder information. Through this process, a personal trainer can monitor muscle movement and assess the performance of the current motion.

3.1.2. Sensor Data Communication and Visualization for Mixed Reality

The developed digital twin models were integrated using the widely used Mixed Reality Tool Kit(MRTK) library in the Unity visualization platform. First, input information, such as the angle and current data, is transmitted and received between the server and the exoskeleton hardware through serial communication (USB and Bluetooth) and wireless communication (TCP/IP environment). This information is then integrated into the digital twin within the Unity environment, enabling the acquisition of complex data such as torque, muscle contraction, and exercise status. Finally, the Unity-driven results are displayed through the HoloLens, which enables MR implementation for enhanced user convenience. Since the HoloLens is a mobile device, it receives data wirelessly using the TCP/IP method. Therefore, the server is responsible for the operation of the Unity environment and the connection between the MID and HoloLens.

© 2023 Wiley-VCH GmbH

2365709x, 2024, 2, Downloaded from https://onlinelibrary.wiley.com/doi/10.1002/admt.202301404 by Kyung Hee University Library, Wiley Online Library on [19/11/2024]. See the Terms and Conditions (https://onlinelibrary.wiley.com/terms-and-conditions) on Wiley Online Library for rules of use; OA articles are governed by the applicable Creative Commons License

3.2. Synchronization of the hUGE Motion and Unity Avatar Posture

The shoulder and elbow rotation axes are aligned with the MID rotation axes to synchronize the Unity avatar's posture and the hUGE motion (Figure S2a, Supporting Information). In this case, the shoulder motion is arranged based on the assumption of three-axis rotation (*x*-*y*-*z*), and the elbow motion is assumed to be one-axis rotation (for *x*-axis) (Figure S2b, Supporting Information). We used an inverse kinematic approach to match the avatar joints and the MID rotation axes (Figure S2c, Supporting Information).

An interactive motion-active skeleton must be implemented through the rigging process to activate an avatar in Unity. The rigged avatar skeleton is implanted in a twisted state along the *x*-*y*-*z* axes from the default pose (i.e., reset pose). The problem of the twisted state commonly occurs during avatar productions. The MID rotation mismatch with the avatar rotation can occur because the MID is designed with the standard *x*-*y*-*z* axis direction as the default pose during the production process. For example, the MID rotates in the *y*-axis vertical plane when lifting a dumbbell using only the elbow, while the avatar moves in a posture that rotates the forearm or twists it to the side rather than lifting the dumbbell. A constraint function applying the inverse kinematics provided by Unity is used to solve this problem. This allows the target object to rotate in the same direction as the reference object, regardless of their coordinate systems in the Unity world coordinate system. In this case, a reference object is assigned to each MID rotation axis and then connected to the avatar's skeleton. As a result, the avatar can accurately reflect and move according to the MID's shoulder (X, Y, and Z) and the elbow's *x*-axis rotation, allowing the correct torque to be transmitted to the MID based on the avatar's posture (Figure S2d, Supporting Information).

The Unity avatar mainly moves through an animator, but the animator only offers movements prerecorded in animation clips. The animation clips have a limitation in reflecting MID movements in real-time. To solve this problem, a constraint component is used to control the movement of the arms. The constraint component controls the avatar's posture and can align the avatar's rig (bone) coordinate axis with the desired coordinate axis. The rotation values of the MID are reflected in the target object of the constraint, and the corresponding part of the avatar is controlled to match the appearance of the target object. This process reflects the avatar's animation and real-time movements separately.

3.3. Calculation of the Tangible Torque Caused by Avatar-Object Interaction in the Metaverse

The torque calculation based on the Unity avatar's posture is determined relative to the vertical plane of the MID joint coordinate axes. This is sequentially defined by the MID joint structure relationship. The MID is connected from the shoulder joint to the elbow joint in the order of the *y*-axis shoulder, *z*-axis shoulder, *x*-axis shoulder, and *x*-axis elbow. In this case, the top shoulder *y*-axis causes coordinate transformations for all the axes below it. To accurately reflect this in the Unity avatar, the reference objects used in the previously mentioned constraint function are set in a parent-child relationship, ensuring the same order is reflected in Unity. We considered that Unity's base coordinate system differs from the standard engineering coordinate system. The vertical upward vector represents the *z*-axis in a typical coordinate system, but the vertical upward vector represents the *y*-axis, and the horizontal rightward vector represents the *x*-axis in Unity. This article explicitly states that descriptions are based on the engineering coordinate system to avoid confusion.

While Unity has a built-in physics engine, the platform does not contain a built-in feature that links physical interactions with torque. Therefore, we designed a script to calculate the torque caused by avatar-object interaction directly. The script's variables include the upper and lower arm length as initial variables, the weight of the object grasped, and the shoulder angle and elbow angle according to the avatar's posture are used for torque calculation. For the shoulder, the angle is calculated according to the parent-child relationship in the order of *z*-*y*-*x* axes according to the design structure of the MID. This means that a change in the angle of the *z*-axis changes the rotation reference axes of *y*, *x*, and the elbow, and a change in the angle of the *y*-axis changes the rotation reference axis of *x* and the elbow. Although the *x*-axis has the elbow as a child relationship, it has the same rotation reference axis direction, so a change in the rotation of *x* can change the position of the elbow, but it does not change the elbow's rotation reference axis.

3.3.1. Generation of Tangible Torques on Joints Due to Gravity Effect of Mass Objects

The torque calculation for lifting an object under the influence of gravity is based on fundamental torque calculations and involves rotating the gravity vector according to the MID's shoulder movement, as shown in Equation (1).

$$R_x = \begin{bmatrix} 1 & 0 & 0 \\ 0 & \cos\theta_1 & -\sin\theta_1 \\ 0 & \sin\theta_1 & \cos\theta_1 \end{bmatrix} \quad R_z = \begin{bmatrix} \cos\theta_2 & -\sin\theta_2 & 0 \\ \sin\theta_2 & \cos\theta_2 & 0 \\ 0 & 0 & 1 \end{bmatrix}$$

$$R_y = \begin{bmatrix} \cos\theta_3 & 0 & \sin\theta_3 \\ 0 & 1 & 0 \\ -\sin\theta_3 & 0 & \cos\theta_3 \end{bmatrix} \tag{1}$$

As mentioned in Section 3.2, the MID and avatar movements undergo rotation in transformation matrices in the order of *y*-*z*-*x* shoulder joints as follows:

$${}^0_3R = \begin{bmatrix} \cos\theta_2\cos\theta_3 & -\sin\theta_2 & \cos\theta_2\sin\theta_3 \\ \cos\theta_1\sin\theta_2\cos\theta_3 + \sin\theta_1\sin\theta_3 & \cos\theta_1\cos\theta_2 & \cos\theta_1\sin\theta_2\sin\theta_3 - \sin\theta_1\cos\theta_3 \\ \sin\theta_1\sin\theta_2\cos\theta_3 - \cos\theta_1\sin\theta_3 & \sin\theta_1\cos\theta_2 & sin\theta_1\sin\theta_2\sin\theta_3 + cos\theta_1\cos\theta_3 \end{bmatrix} \tag{2}$$

© 2023 Wiley-VCH GmbH

2365709x, 2024, 2, Downloaded from https://onlinelibrary.wiley.com/doi/10.1002/admt.202301404 by Kyung Hee University Library, Wiley Online Library on [19/11/2024]. See the Terms and Conditions (https://onlinelibrary.wiley.com/terms-and-conditions) on Wiley Online Library for rules of use; OA articles are governed by the applicable Creative Commons License

Considering the avatar holding an object, the torque calculation is determined by the cross-product of the distance vector from the object to the reference axis point and the object's gravity vector. In this case, the gravity vector always points vertically downward based on the world coordinate system, and it is projected onto the vertical plane of the axis where the torque calculation occurs to determine the gravity vector. For example, when lifting a dumbbell to 90°, using only the elbow in the basic posture without shoulder rotation, the torque generated at the elbow is calculated since the gravity vector is parallel to the vertical plane of the elbow reference axis (elbow x-axis). However, when the elbow is spread 30° (if $\theta_3 = 30°$, $\theta_1 = \theta_2 = 0°$, 30° rotation based on the shoulder y-axis), the vertical plane of the elbow reference axis is also rotated 30°. Since the object's gravity vector still points vertically downward in this case, its impact on the elbow changes. To solve this, the cross-product is performed using the transformed vector obtained by projecting the object's gravity vector onto the reference axis vertical plane, thereby calculating the transformed elbow torque. The following formula shows the gravity vector change according to Unity's hierarchical structure. In this case, the vertical plane concerning the elbow reference axis is the z–y plane. After the shoulder movement, the torque generated at the elbow is calculated using the remaining z value, excluding the x component of the rotated gravity vector.

In Unity, all objects can have a unique weight set through the rigid body component. When the avatar grabs the object through VR interaction, the weight set on the rigid body component and the torque caused by the joint angle is calculated. The calculation of torque caused by gravity on each joint is done by expressing the vertical plane of each joint, the weight vector of the object held by gravity, the distance vector between the center of the joint and the point of holding, and by then taking the cross product of each vector to calculate the torque on the joint. This is simply the algorithm of calculating the torque on a plane, but it can easily represent the change in torque caused by the change in posture on each joint. For example, when the initial elbow is bent at 90°, the gravity vector is drawn in the shoulder's Z-axis, X-axis, and Elbow-axis plane, but it cannot be drawn in the Y-axis plane. However, when it rotates 90° inward on the z-axis, the gravity vector is not drawn on the x-axis or Elbow-axis plane but on the y-axis plane.

3.4. Loaded Tooth Contact Analysis (LTCA) Results of the Fabricated Reduction Gearbox for Tangible Torque Generation and Feedback

There could be various data streams from the LTCA simulation results, such as safety factors, transmission error, bearing displacement, shaft deflection, etc. This work focuses on the safety factors because the LTCA simulation aims to verify the strength of the designed reduction gearbox, especially of the tooth. The LTCA is conducted for all mating gear pairs, such as sun gear, planetary gears, and annulus gears, and the first and second stages. The simulations conducted for the load cases are explained in Section 2.2. The contact stresses for the tooth flank of gearsets are calculated based on Hertzian contact theory. The bending and contact safety factors are calculated using ISO 6336 standards. The calculated safety factors are summarized in Table S4 (Supporting Information) for load case 1 and Table S5 (Supporting Information) for load case 2. Because load case 2 has higher torque than load case 1, the overall safety factors of load case 2 are lower than load case 1. However, the lowest safety factor is the bending safety factor of the planet gears of stage one, and it is 10.14, which means that the maximum stress is almost 10% of the allowable stress. Consequently, the design of the reduction gearbox is verified through the LTCA simulation because the results mean it has sufficient structural strength for the operating conditions (See Figure S4, Supporting Information).

3.5. Electromyographic (EMG) Sensing Results for Exercise Efficacy Testing According to Metaverse Feedback and Communication While in Motion

EMG sensors were attached to the skin over the biceps, and EMG signals were acquired while moving the arm from 0° to 150° (**Figure 3a**). EMG signal measurements were conducted under three conditions: before and after wearing the MID and while wearing only the Oculus (Figure 3b). The time zone (or period, "TZ") displays the flow of bicep movement. For example, in the time period at 2.5 kg, the EMG value when measured with the Oculus (green) shows virtually no muscle usage, while the value when wearing the MID (blue) is similar to the EMG value of bicep movement without wearing the MID (red) (Figure 3c). The EMG data by weight show that the EMG values of bicep movements without wearing the MID and while wearing the MID are similar (Figure 3d–i). The weight-specific EMG graph should ideally have an up-and-down vibration-like graph shape, but it was made visually more accessible by giving it a value of 100 through RMS conversion. In addition, the graph shows that the EMG values during the actual bicep exercise and while wearing the MID are similar (Figure 3d–ii). The graph of torque values according to the current of the motor combined with the gearbox shows that if the virtual weight setting exceeds 5 kg, the motor rotation and gear ratio cause jamming within the gearbox due to the designed gear ratio (= 47.667) of the gearbox for providing feedback. This is because the maximum torque is 0.2 N m when 10 A is applied based on the elbow, and since the arm length on MID is 0.25 m, it is calculated as 38.134 N, corresponding to 4 kg. Therefore, caution is needed as excessive force can be applied when wearing MID due to the gearbox jamming caused by the motor's rotational load. In the RMS converted graph of Figure 3d–ii, the initial value of the time zone (TZ) 1 at 5 kg is observed to spike due to the jamming that occurred, as explained earlier. After the initial jamming, it stabilizes and maintains a steady state (Figure 3e).

The EMG results must have clear logic for why such data were obtained for each experiment, and the EMG data results must be discussed in terms of how they will help actual rehabilitation. For example, EMG values similar to actual movements were observed when wearing MID compared to the previously used Oculus equipment. This result indicates a higher immersion level than Oculus through EMG values. This showed that muscle usage regarding actual and virtual object weights was similar, enabling rehabilitation without being limited by location and needing multiple dumbbells. Furthermore, using MID for strength training exercises can provide optimal exercise intensity by controlling the weight or resistance. This allows for strengthening muscles and

© 2023 Wiley-VCH GmbH

2365709x, 2024, 2, Downloaded from https://onlinelibrary.wiley.com/doi/10.1002/admt.202301404 by Kyung Hee University Library, Wiley Online Library on [19/11/2024]. See the Terms and Conditions (https://onlinelibrary.wiley.com/terms-and-conditions) on Wiley Online Library for rules of use; OA articles are governed by the applicable Creative Commons License

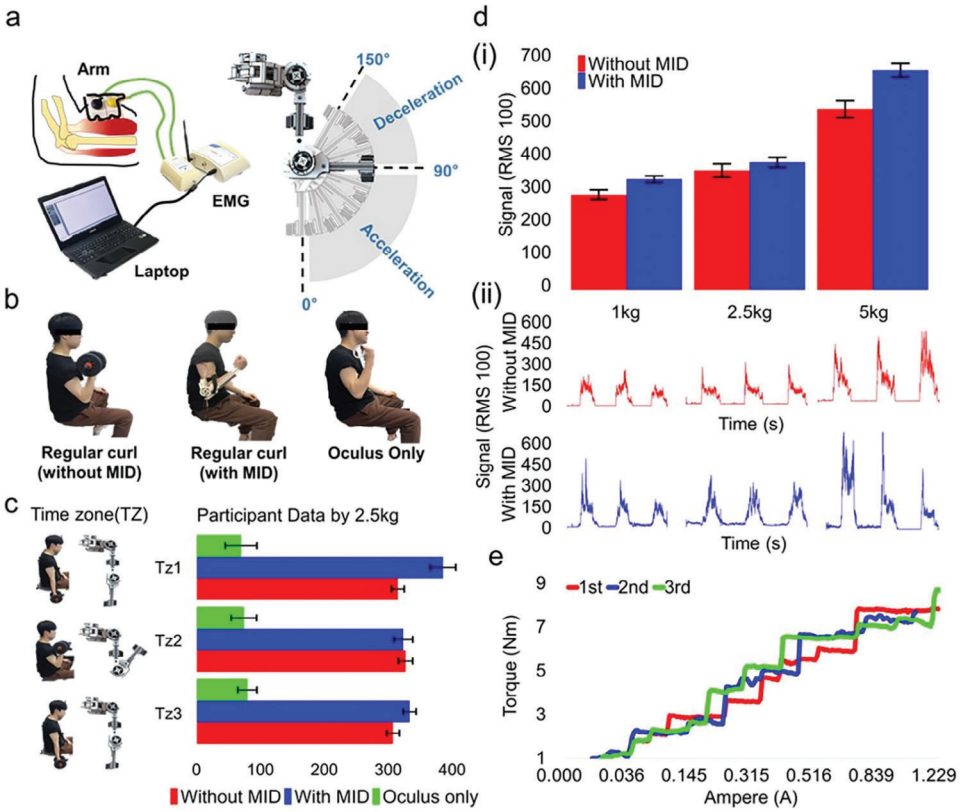

Figure 3. Electromyographic experimental results for the hybrid XR biceps motion while in operation. a) Experimental method and angle range of EMG experiments. b) Experimental motions (with and without wearing the device and Oculus). c) Diagram explaining each time zone (TZ) and mean values of each section for participants. d) i) Relationship between EMG values for 1, 2.5, and 5 kg, and ii) EMG graph of each section for 1, 2.5, and 5 kg with and without wearing the device. e) Measured torque of the motor attached to the gearbox.

adjusting exercise time for continuous training, which in turn helps improve muscular endurance. Moreover, rehabilitation using MID is expected not only for therapeutic purposes but also to allow users to have new experiences in the virtual world, potentially reducing the boredom and burden of rehabilitation.

3.6. Thermographic Imaging Analysis Results for Checking the User's Skin Temperature Safety While Using the Metaverse Wearable

A thermal imaging experiment was conducted to measure the thermal images at specific locations during the MID bicep movement using a thermal imaging device by FLIR(FLIR E6-XT wifi, USA) (**Figure** 4a). While maintaining the maximum angle of 150° for the MID, a continuous load was applied for ≈35 s to overload the BLDC motor. As a result, the maximum temperature measured at the motor part was 80.5°C, and the maximum temperature observed at the body contact part was 27.5°C (Figure 4b). An experiment was conducted to measure the actual heat generated while in operation by observing skin temperature changes according to the MID angle change by the curl movement of the elbow (Figure 4c). For example, three reciprocating exercises were performed from 0 to 45 s, and the temperature increased linearly and reached saturation at 40 s (Figure 4d). The temperature change during the curl movement is rapid, and the temperature increases due to heat transfer even after the curl movement. Low-temperature thermal imaging refers to burns that occur when exposed to temperatures above 40°C for more than one hr, which is lower than the temperature that typically causes burns.

3.7. Overlapped Layout Visual Performance of Anatomical Digital Twin Model with the Metaverse Exoskeleton for Hololens-based MR Feedback

The sensor data of the MID is used to represent the digital twin and metaverse through Unity. We measured the visual delay in wireless communication environments for real movement and found it to be less than 10% of a single exercise execution time or ≈200 ms. The latency during server-client communication is ≈10 ms, with most of the delay stemming from the hardware's inherent processing speed. This result will be further improved depending on hardware performance and the communication environment (**Figure** 5a). It should be noted that even a little latency can make people feel sick or dizzy in VR, as the signals from the visual cortex do not align with those from the inner ear.

Furthermore, it may be helpful to import the Unity code into a headset format. It is a reasonable assumption that such CPU/GPU/headset-integrated AR/VR devices will become less expensive. The visualized digital twin results provide the torque and angle information of the MID motor and a virtual anatom-

© 2023 Wiley-VCH GmbH

2365709x, 2024, 2, Downloaded from https://onlinelibrary.wiley.com/doi/10.1002/admt.202301404 by Kyung Hee University Library, Wiley Online Library on [19/11/2024]. See the Terms and Conditions (https://onlinelibrary.wiley.com/terms-and-conditions) on Wiley Online Library for rules of use; OA articles are governed by the applicable Creative Commons License

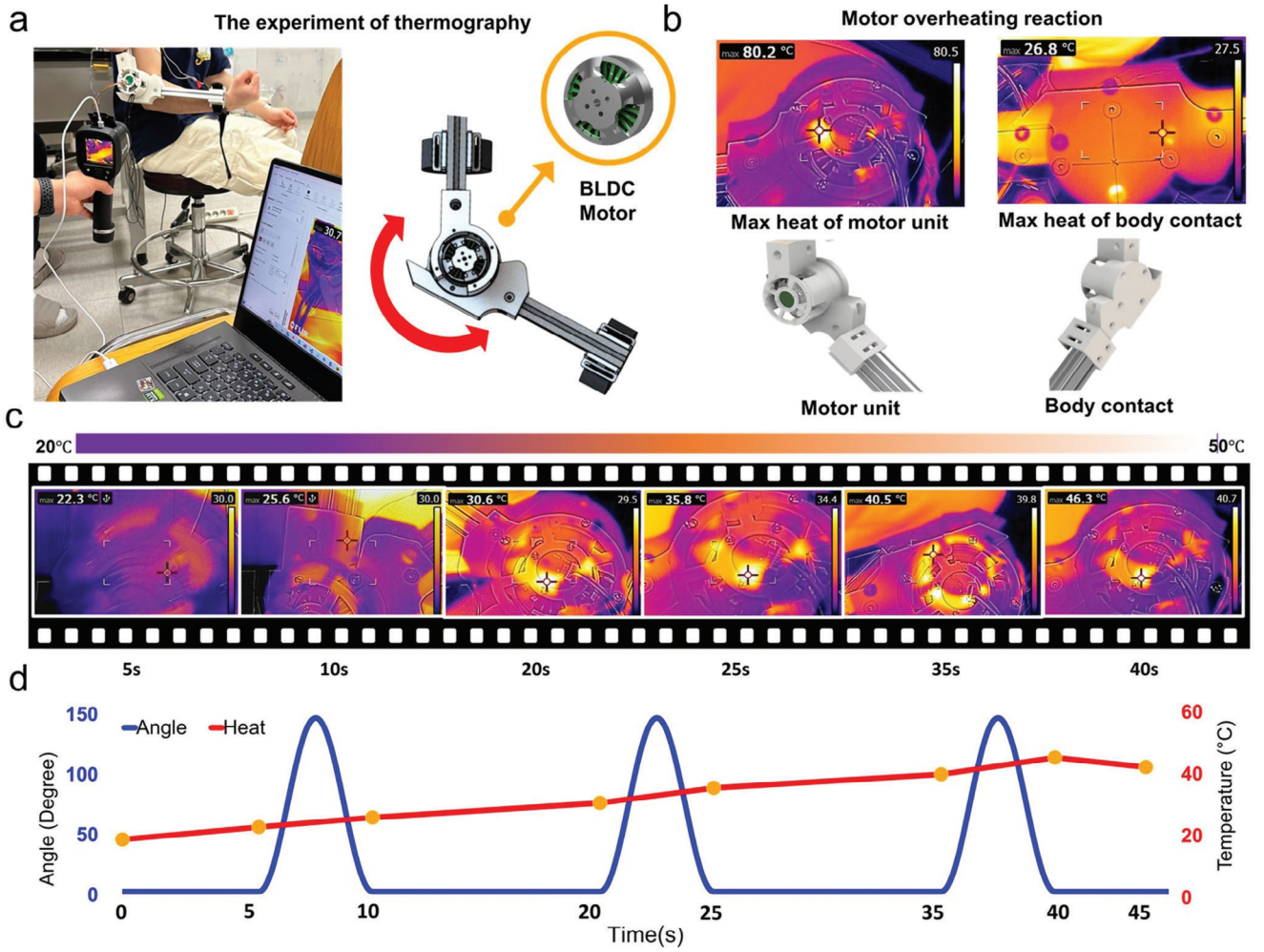

Figure 4. Thermographic experimental results for motor heating effect while in operation. a) Photograph of the experimental setup for thermographic measurement for thermal imaging during these two movements. b) Comparison of the temperature between motor and body contact parts while the BLDC motor is overloaded by continuously applying a load to maintain the maximum angle (for actual motor and body contact parts). c) Sequential photographs of motor temperature change from 0 to 45 s while in operation, and d) Graph for motor temperature change corresponding to the angles of MID operation versus time.

ical model (Figure 5b). The angle and torque data are used for monitoring the mechanical state of the MID, and the anatomical model can be utilized to provide customized coaching by experts, such as personal trainers, based on muscle movement; observing muscle modeling visualization by a supervisor can increase the accuracy of exercise movements during the rehabilitation process and potentially enhance the physical therapy effects instead of simply performing movements.[32] The correspondence of the digital twin model according to the angle of the MID was visualized (Figure 5c).

Angle data represents the current state of the mechanical and anatomical models. Angles are assigned to each joint degree of freedom to make the digital twin move identically to its physical counterpart. In this process, the coordinate system is transformed through a transformation matrix, as in Equation (3), with the rotation point of each joint as the origin. The regressed value from the experimentally measured current-torque diagram calculates the torque generated by the MID device according to the weight. The digital twin results can monitor muscle movement, equipment status, and other aspects during the trainee's exercise.

$$\begin{Bmatrix} x' \\ y' \\ z' \\ 1 \end{Bmatrix} = \begin{bmatrix} s_x r_{11} & r_{12} & r_{13} & t_x \\ r_{21} & s_y r_{22} & r_{23} & t_y \\ r_{31} & r_{32} & s_z r_{33} & t_z \\ 0 & 0 & 0 & 1 \end{bmatrix} \begin{Bmatrix} x \\ y \\ z \\ 1 \end{Bmatrix} \quad (3)$$

The transformation matrix elements consist of rotation, translation, and scale. The rotation component (r) can be calculated from Euler angles. The translation component (t) is calculated as the value for moving the origin. The scale component (s) allows adjusting the object's size within the coordinate system for each axis direction. By multiplying the transformation matrix by the original coordinates (xyz), the coordinate values in the modified coordinate system can be calculated. Figure 5c shows a scene captured through the "*HoloLens*" during the trainee's curl exercise.

© 2023 Wiley-VCH GmbH

2365709x, 2024, 2, Downloaded from https://onlinelibrary.wiley.com/doi/10.1002/admt.202301404 by Kyung Hee University Library, Wiley Online Library on [19/11/2024]. See the Terms and Conditions (https://onlinelibrary.wiley.com/terms-and-conditions) on Wiley Online Library for rules of use; OA articles are governed by the applicable Creative Commons License

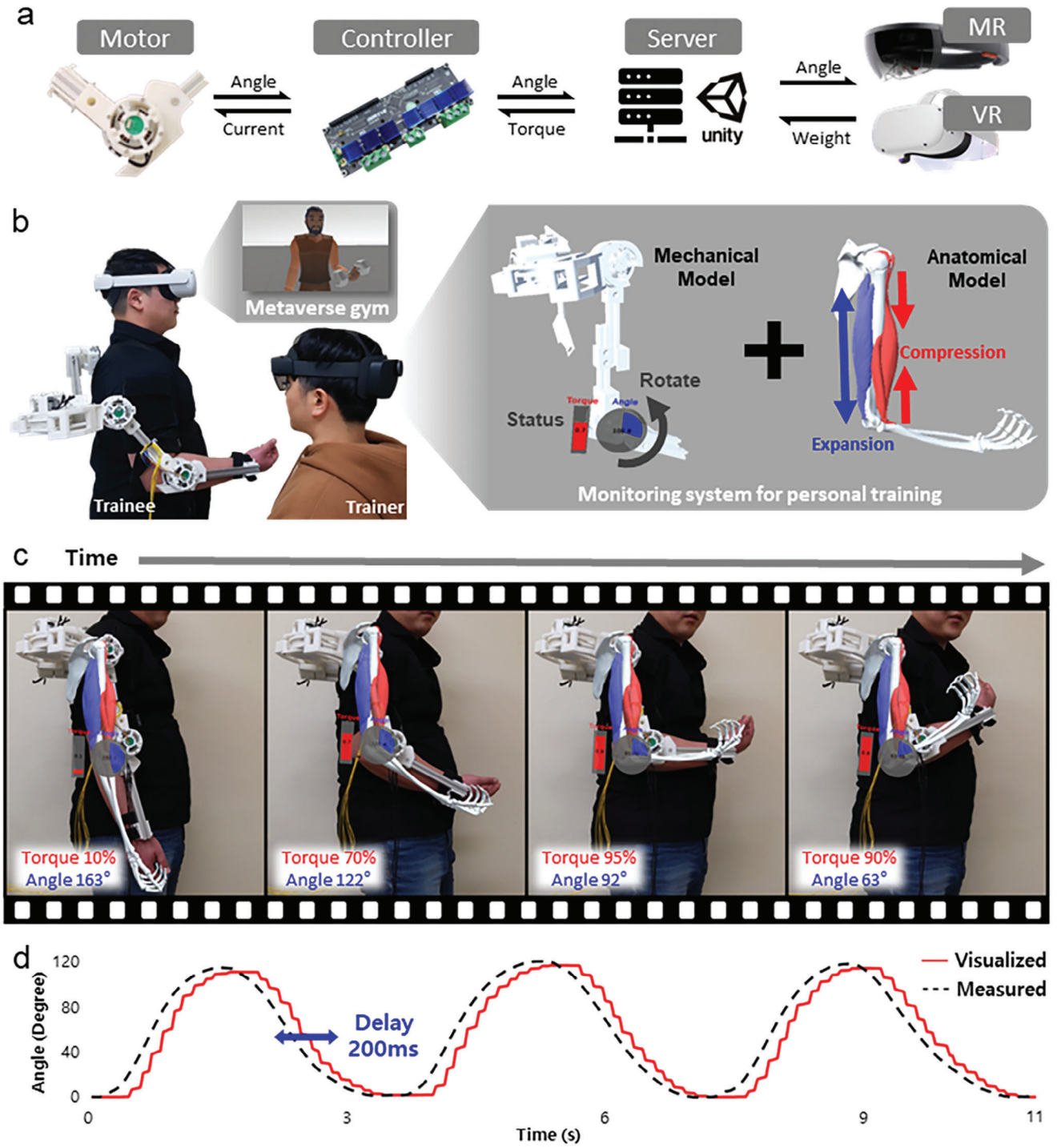

Figure 5. Demonstration results of the hybrid XR-metaverse wearable device while in operation. a) Schematic illustration of data communication from the hUGE sensor to a combined Metaverse and digital twin. b) The scenario enables the trainer and trainee to interact using extended reality (XR) devices. The trainee can track motion status in the real world and the metaverse. At the same time, the trainer can monitor the trainee's motion condition through a combination of mechanical and anatomical models. c) Time-lapse photographs of the hUGE digital twin operation via Hololens according to the trainee's upper-arm motions from a toggle position (fully stretched) to full flexion (fully folded). d) The differences between the measured and visualized angles during the three movements. The angle of the digital twin has an average delay of ≈200 ms, less than 10% of the time of a single movement.

© 2023 Wiley-VCH GmbH

2365709x, 2024, 2, Downloaded from https://onlinelibrary.wiley.com/doi/10.1002/admt.202301404 by Kyung Hee University Library, Wiley Online Library on [19/11/2024]. See the Terms and Conditions (https://onlinelibrary.wiley.com/terms-and-conditions) on Wiley Online Library for rules of use; OA articles are governed by the applicable Creative Commons License

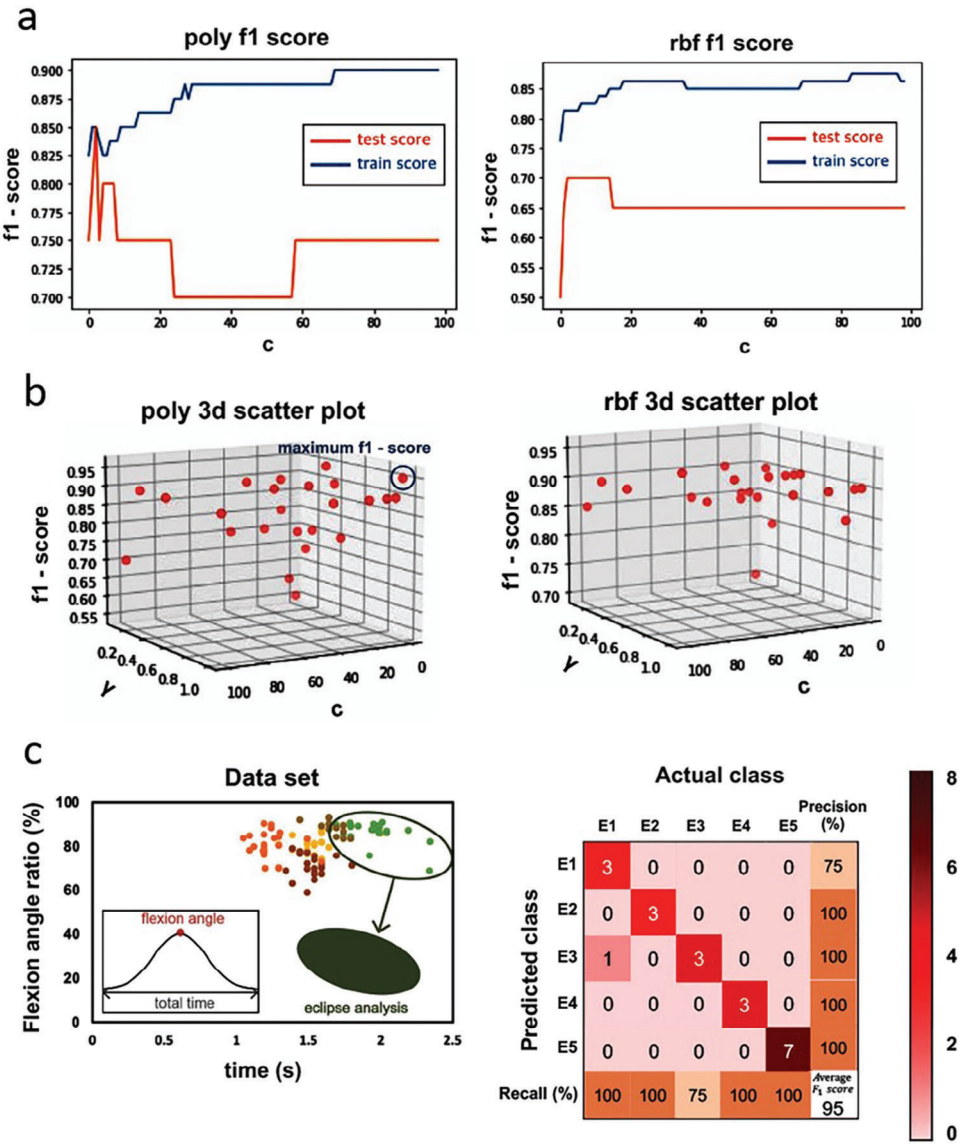

Figure 6. Support vector machine analysis of the biceps motion cycle using the hybrid XR-metaverse wearable. a) Comparison of f1 score values based on poly and radial basis (RBF) function, b) Scatter plots of f1 score functions according to penalty parameters (c, γ), and c) Classification by confusion matrix (including recall and precision values) according to the normalized flexion angle ratio. The wider the data clusters form (i.e., eclipse), the more time the biceps have to reach the target object (as indicated by the oblique angle according to time).

The MID device's motor angle and generated torque can be overlapped and checked in real-time (Figure 5d). The torque is displayed as a ratio of the maximum torque generated in each weight case, and the angle represents the elbow joint's angle. These results showed that the maximum torque was generated when the angle reached 90°. The trainer can use this information to understand the load and exercise status in real-time.

3.8. Haptic Fidelity and Versatility Evaluation

Haptic feedback devices in the metaverse are crucial for providing users with realism and versatility. Consequently, we analyzed the realism and versatility of the fabricated device in this study. We employed the haptic fidelity rule to define the haptic feedback device's realism and versatility.[33]

$$\text{Haptic Fidelity (HF)} = \overline{\mathbf{FF}} \times \mathbf{e}^{-0.0027(\sum \mathrm{LF}^2)^2} \quad (4)$$

where $\overline{FF}$, the average value of the fundamental factors (X_F), and LF, the value of the limiting factors (X_L)

Haptic fidelity comprises 14 elements: body position, body area, stimulus, size, sensory preservation, dependence, discriminability, degrees of freedom, hardware precision, hardware latency, side effects, constraints, software precision, and software latency. Among these elements, dependence, hardware latency, side effects, constraints, software latency, and discriminability are

© 2023 Wiley-VCH GmbH

2365709x, 2024, 2, Downloaded from https://onlinelibrary.wiley.com/doi/10.1002/admt.202301404 by Kyung Hee University Library, Wiley Online Library on [19/11/2024]. See the Terms and Conditions (https://onlinelibrary.wiley.com/terms-and-conditions) on Wiley Online Library for rules of use; OA articles are governed by the applicable Creative Commons License

potentially limiting factors, depending on the scenario. The remaining eight elements are fundamental factors.

The haptic fidelity and versatility range can be defined between 0 and 4. Fundamental factors (X_F) contribute to increased realism, whereas limiting factors (X_L) reduce realism. Higher realism is achieved when fundamental factors are closer to four and limiting factors are closer to 0. Values representing the haptic fidelity value based on the sum of the limiting factors and fundamental factors can define that the squares of the limiting factors on the *x*-axis range from 1 to 11 (Figure S3a, Supporting Information). The graph represents three cases where the sum of the fundamental factors is 23, 27, and 31. HF realism has a minimum value of 2.07 and a maximum of 3.86. The MID's range of realism and versatility is expressed, with realism and versatility having a maximum value of four. The MID has a median value of (2.07, 3) for realism and versatility (Figure S3b, Supporting Information). Note that the haptic fidelity was compared regarding the existing protocol, "Haptic fidelity framework," defining the factors of realistic haptic feedback for virtual reality.[33]

3.9. Support Vector Machine (SVM)-Based Data Analysis for Subtle Movement Variations

Figure 6 illustrates the results of classification using the SVM method. Figure 6a represents the appearance of the f1 score values for the training and test data as a function of the *c* value. As the *c* value increases, the accuracy of the training data improves, while the test data exhibits an increasing pattern before decreasing. Furthermore, Figure 6b shows the test data's accuracy depending on both *c* and gamma values. During this phase, it was observed that the accuracy was higher when using a poly kernel, and the highest accuracy was attained when *c* was five and gamma was 0.25. At this point, the f1 score for the training data was 0.8375, and the test data was 0.85, indicating high accuracy and a suitable model was formed using these variable values. Figure 6c depicts the distribution of instantaneous bending angles and time data for one cycle performed by the initial five participants. The 20 consecutive bending-stretching movements provided repetitive data, enabling the diagnosis of the participant's condition through the distribution pattern.

Additionally, the right side of Figure 6c presents a confusion matrix for evaluating the classification model's prediction results, revealing accurate classification through an average f1 score value of 0.95. These results facilitated accurately classifying participants with similar muscle strength and movement. The method of learning and prediction through participant data is anticipated to establish standards and diagnostics and potentially optimize MR/VR routines for rehabilitation or muscle strength measurement. Note that the context and the specifics of "bending and stretching" experiments and the meaning of "distribution pattern of participants" were inferred from the given text. Adjustments might be necessary if the context differs.

4. Conclusion

This study highlights the need for a hybrid anatomical digital twin incorporated wearable interface with high-dimensional input/output capabilities to implement metaverse environmental interactions and their real-time feedback. We also present a novel design of an upper limb exoskeleton as a proof-of-concept demonstration that can perform tangible torque feedback between real-world and metaverse environments for remote healthcare monitoring applications. Several experiments have demonstrated that the motion-interactive actuator's response characteristics are good and that mechanical feedback is well reflected. Furthermore, we showed that this approach has superior human-informed model guidance to other VR devices through haptic fidelity criteria. This approach can be potentially helpful in providing a new way for healthcare professionals to monitor and assist patients under a hybrid metaverse-XR environment in the post-pandemic era.

Supporting Information

Supporting Information is available from the Wiley Online Library or from the author.

Acknowledgements

Minhyeok Ha and Jihun Lee equally contributed to this work. This work was financially supported by the National Research Foundation of Korea (NRF) grant funded by the Ministry of Science and ICT, Korea (2021R1F1A1048603 and 2020R1A2C1006842)

Conflict of interest

The authors declare no conflict of interest.

Author Contributions

M.H. and J.L. contributed equally to this work. W.G.L. conceived the project and led the initiative of collaborative research. M.H., M.L., J.S., and J.H.L. designed and fabricated the upper-arm guided exoskeletal system and performed motion experiments. M.H. developed the metaverse environment by using Unity. M.H. and J.H.L. performed graphical data analysis and performed electromyogram (EMG) experiments. J.H.L. performed FLIR-based thermographic experiments. Y.C. developed the digital twin system and incorporated the upper-arm muscle model over the system in an XR format. H.P. performed the LTCA analysis of the reduction gear set. J.L. performed support vector machine analysis. S.C. performed the haptic fidelity analysis. J.K. supervised the digital twin and LTCA parts of the work. K.K. and W.G.L. supervised all aspects of the work. All the authors discussed ideas and results and contributed to writing the manuscript.

Data Availability Statement

The data that support the findings of this study are available in the supplementary material of this article.

Keywords

digital twins, metaverse wearables, personalized rehabilitation, remote healthcare monitoring, tangible torques

Received: August 27, 2023
Revised: October 30, 2023
Published online: December 7, 2023

© 2023 Wiley-VCH GmbH

2365709x, 2024, 2, Downloaded from https://onlinelibrary.wiley.com/doi/10.1002/admt.202301404 by Kyung Hee University Library, Wiley Online Library on [19/11/2024]. See the Terms and Conditions (https://onlinelibrary.wiley.com/terms-and-conditions) on Wiley Online Library for rules of use; OA articles are governed by the applicable Creative Commons License

[1] A. M. Briggs, J. E. Jordan, D. Kopansky-Giles, S. Sharma, L. March, C. H. Schneider, S. Mishrra, J. J. Young, H. Slater, *Global Health Res. Policy* **2021**, *6*, 24.
[2] A. Langer, L. Gassner, A. Flotz, S. Hasenauer, J. Gruber, L. Wizany, R. Pokan, W. Maetzler, H. Zach, *NPJ Parkinson's Dis.* **2021**, *7*, 25.
[3] K. Kim, W. G. Lee, *Small Methods* **2023**, *7*, 2200979.
[4] C. Adans-Dester, N. Hankov, A. O'brien, G. Vergara-Diaz, R. Black-Schaffer, R. Zafonte, J. Dy, S. I. Lee, P. Bonato, *NPJ Digital Med.* **2020**, *3*, 121.
[5] X. Li, L. Liu, X. Wang, Y. S. Ok, J. A. W. Elliott, S. X. Chang, H.-J. Chung, *Sci. Rep.* **2017**, *7*, 1685.
[6] P. D. Marasco, J. S. Hebert, J. W. Sensinger, D. T. Beckler, Z. C. Thumser, A. W. Shehata, H. E. Williams, K. R. Wilson, *Sci. Rob.* **2021**, *6*, eabf3368.
[7] C. G. Canning, N. E. Allen, E. Nackaerts, S. S. Paul, A. Nieuwboer, M. Gilat, *Nat. Rev. Neurol.* **2020**, *16*, 409.
[8] O. N. Beck, M. K. Shepherd, R. Rastogi, G. Martino, L. H. Ting, G. S. Sawicki, *Sci. Rob.* **2023**, *8*, eadf1080.
[9] P. Slade, M. J. Kochenderfer, S. L. Delp, S. H. Collins, *Nature* **2022**, *610*, 277.
[10] K. L. Poggensee, S. H. Collins, *Sci. Rob.* **2021**, *6*, eabf1078.
[11] C. Siviy, L. M. Baker, B. T. Quinlivan, F. Porciuncula, K. Swaminathan, L. N. Awad, C. J. Walsh, *Nat. Biomed. Eng.* **2022**, *7*, 456.
[12] C. Li, D. Liu, C. Xu, Z. Wang, S. Shu, Z. Sun, W. Tang, Z. L. Wang, *Nat. Commun.* **2021**, *12*, 2950.
[13] S. Crea, M. Nann, E. Trigili, F. Cordella, A. Baldoni, F. J. Badesa, J. M. Catalán, L. Zollo, N. Vitiello, N. G. Aracil, S. R. Soekadar, *Sci. Rep.* **2018**, *8*, 10823.
[14] M. Zhu, Z. Sun, T. Chen, C. Lee, *Nat. Commun.* **2021**, *12*, 2692.
[15] S. Ke, F. Xiang, Z. Zhang, Y. Zuo, *Proc. CIRP* **2019**, *83*, 753.
[16] K. Kim, H. Yang, J. Lee, W. G. Lee, *Adv. Sci.* **2023**, *10*, 2303234.
[17] J. Xiong, E.-L. Hsiang, Z. He, T. Zhan, S.-T. Wu, *Light Sci. Appl.* **2021**, *10*, 216.
[18] G. Wang, A. Badal, X. Jia, J. S. Maltz, K. Mueller, K. J. Myers, C. Niu, M. Vannier, P. Yan, Z. Yu, R. Zeng, *Nat. Mach. Intell.* **2022**, *4*, 922.
[19] K. Liu, Y. Gao, A. Abdelrehem, L. Zhang, X. Chen, L. Xie, X. Wang, *Sci. Rep.* **2021**, *11*, 10043.
[20] S. A. Niederer, M. S. Sacks, M. Girolami, K. Willcox, *Nat. Comput. Sci.* **2021**, *1*, 313.
[21] J.-H. Lee, H.-L. Lee, I.-Y. Park, S.-W. On, S.-H. Byun, B.-E. Yang, *Sci. Rep.* **2023**, *13*, 10603.
[22] R. Yilmaz, A. Winkler-Schwartz, N. Mirchi, A. Reich, S. Christie, D. H. Tran, N. Ledwos, A. M. Fazlollahi, C. Santaguida, A. J. Sabbagh, K. Bajunaid, R. Del Maestro, *NPJ Digital Med.* **2022**, *5*, 54.
[23] P. Falkowski, T. Osiak, J. Wilk, N. Prokopiuk, B. Leczkowski, Z. Pilat, C. Rzymkowski, *Sensors* **2023**, *23*, 911.
[24] K. P. Venkatesh, M. M. Raza, J. C. Kvedar, *NPJ Digital Med.* **2022**, *5*, 150.
[25] R. Laubenbacher, A. Niarakis, T. Helikar, G. An, B. Shapiro, R. S. Malik-Sheriff, T. J. Sego, A. Knapp, P. Macklin, J. A. Glazier, *NPJ Digital Med.* **2022**, *5*, 64.
[26] H. Yu, S. Huang, G. Chen, Y. Pan, Z. Guo, *IEEE Transact. Robot.* **2015**, *31*, 1089.
[27] T. Elery, S. Rezazadeh, C. Nesler, R. D. Gregg, *IEEE Transact. Robot.* **2020**, *36*, 1649.
[28] T.-H. Huang, S. Zhang, S. Yu, M. K. Maclean, J. Zhu, A. Di Lallo, C. Jiao, T. C. Bulea, M. Zheng, H. Su, *IEEE Transact. Robot.* **2022**, *38*, 1442.
[29] H. Matsuki, K. Nagano, Y. Fujimoto, *IEEE/ASME Transact. Mechatron.* **2019**, *24*, 2661.
[30] H. Dong, Z.-Y. Liu, L.-L. Duan, Y.-H. Hu, *PLoS One* **2018**, *13*, e0198677.
[31] N. Mitsuhashi, K. Fujieda, T. Tamura, S. Kawamoto, T. Takagi, K. Okubo, *Nucleic. Acids Res.* **2009**, *37*, D782.
[32] J. Zhu, Y. Lei, A. Shah, G. Schein, H. Ghaednia, J. Schwab, C. Harteveld, S. Mueller, In *Adjunct Proceed. of the 35th Ann. ACM Sympos. on User Interface Software and Technology*, Association for Computing Machinery, Bend, OR **2022**, *110*, 1.
[33] T. Muender, M. Bonfert, A. Reinschluessel, R. Malaka, T. Doring, In *Proceed. of the 2022 CHI Conf. on Human Factors in Computing Systems*, Association for Computing Machinery, New Orleans, LA **2022**, *431*, 1.

© 2023 Wiley-VCH GmbH

2365709x, 2024, 2, Downloaded from https://onlinelibrary.wiley.com/doi/10.1002/admt.202301404 by Kyung Hee University Library, Wiley Online Library on [19/11/2024]. See the Terms and Conditions (https://onlinelibrary.wiley.com/terms-and-conditions) on Wiley Online Library for rules of use; OA articles are governed by the applicable Creative Commons License